

Learning Visual Hierarchies in Hyperbolic Space for Image Retrieval

Ziwei Wang^{1,2*} Sameera Ramasinghe^{1*} Chenchen Xu¹
 Julien Monteil¹ Loris Bazzani¹ Thalaisyasingam Ajanthan^{1*}

¹Amazon ²Australian National University

Abstract

Structuring latent representations in a hierarchical manner enables models to learn patterns at multiple levels of abstraction. However, most prevalent image understanding models focus on visual similarity, and learning visual hierarchies is relatively unexplored. In this work, for the first time, we introduce a learning paradigm that can encode user-defined multi-level complex visual hierarchies in hyperbolic space without requiring explicit hierarchical labels. As a concrete example, first, we define a part-based image hierarchy using object-level annotations within and across images. Then, we introduce an approach to enforce the hierarchy using contrastive loss with pairwise entailment metrics. Finally, we discuss new evaluation metrics to effectively measure hierarchical image retrieval. Encoding these complex relationships ensures that the learned representations capture semantic and structural information that transcends mere visual similarity. Experiments in part-based image retrieval show significant improvements in hierarchical retrieval tasks, demonstrating the capability of our model in capturing visual hierarchies.

1. Introduction

Humans organize knowledge of the world into hierarchies [27] for efficient knowledge management. Developing models that encode such hierarchies is

* work done while at Amazon

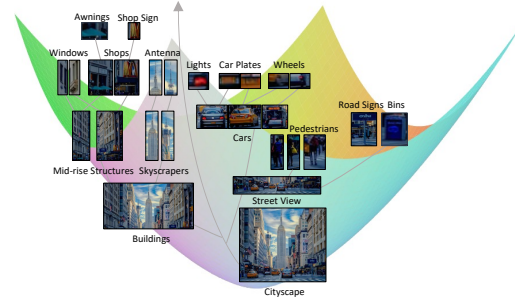


Figure 1. **An illustration of part-based image hierarchy organized in hyperbolic space.** At the highest level, we see the urban environment, composed of buildings, streets, and sky. Zooming in, we find the building category, which further divides into skyscrapers, mid-rise structures, and more. Each of them has its own visual elements, which in turn can be decomposed into sub-elements.

crucial for creating systems with holistic world understanding aligned with human perception. While this topic spans various modalities, we focus on encoding hierarchies in the visual domain. For many large image datasets, objects can be organized according to latent hierarchies [27], as evidenced by power law distributions [35]. However, most prevalent image understanding models [5, 15–17, 37] focus on preserving visual similarity, and consequently, learning hierarchies in the visual domain remains relatively unexplored. These limitations hinder models’ ability to generalize to tasks requiring hierarchical reasoning such as understanding scenes, object parts, and their interactions at multiple levels of abstraction. We illustrate in Fig. 1 an example that shows the complexity of a visual hier-

archy where elements share similarities both within and across categories.

Recent works have demonstrated the utility of hyperbolic representation spaces for capturing hierarchical relationships in an unsupervised setting [7, 31, 33]. This *emergent* latent structure is appealing; nevertheless, meaningful hierarchies are often task and data dependent, and aligning model behavior with such human-defined hierarchies is essential for many applications. To this end, we introduce a learning paradigm that can encode multi-level hierarchies as entailment pairs in hyperbolic space. As a concrete example, we first define a general part-based image hierarchy using object and part level classification annotations within and across images. Then, we introduce a model capable of structuring the latent space to preserve the defined hierarchy using only image/object level information. To our knowledge, we are the first to encode multi-level complex visual hierarchies without relying on explicit hierarchical labels or additional modalities. Finally, we introduce an evaluation metric to effectively measure hierarchical image retrieval.

Note that, hierarchy is an asymmetric relationship and has a high branching factor (see Fig. 1). To this end, we adopt the hyperbolic geometry as it provides a continuous approximation of such tree-like structures [27, 36]. To enforce the hierarchy, we break it into pairwise entailment relationships between images, objects, and parts, at multiple levels within an image as well as across images at category level. For pairwise entailment (asymmetric), we adapt the recently proposed angle-based asymmetric distance metric [33] within the contrastive learning paradigm, and extend it to handle cases with multiple positive relationships. In contrast to symmetric distances such as the inner-product used in [12, 21, 28], this angle-based distance offers an additional degree of freedom along the radial axis to form emergent structures in the latent space.

For experimentation, we build a dataset of visual hierarchies using the bounding box annotations of OpenImages [24]. Our dataset includes entailment relationships between scenes, objects, and parts, within a single image as well as across images at the category level. Similarly, for hierarchical

retrieval evaluation, we use the full training set to create ground truth hierarchy trees per scene/object. Additionally, we design a metric for evaluating hierarchical retrieval based on the optimal transport distance between the label distribution of the retrieval set and ground truth label distribution within the hierarchy tree. Combined with Recall@k metrics, this demonstrates that our method captures semantic and structural information, transcending mere visual similarity. Furthermore, to the best of our knowledge, our model is the first to generalize to out-of-domain image hierarchies, achieving strong performance on unseen and out-of-domain datasets.

Our contributions can be summarized as follows:

- To our knowledge, for the first time, we introduce a new learning paradigm to effectively encode user-defined multi-level complex visual hierarchies in hyperbolic space that does not require explicit hierarchical labels.
- We adapt a contrastive loss using hyperbolic angle-based distance metric to enforce pairwise entailment relationships, and empirically demonstrate that pairwise entailment is sufficient to learn complex visual hierarchies.
- We introduce an optimal transport based evaluation metric to measure hierarchical image retrieval performance.
- We demonstrate superior generalization capabilities of our model beyond the user-defined hierarchies via out-of-domain unseen data evaluation and ablation experiments.

2. Preliminaries

We briefly review essential concepts in hyperbolic geometry here. We refer the reader to [34] for a comprehensive treatment. Hyperbolic spaces are Riemannian manifolds with constant negative curvature and are fundamentally different from Euclidean or spherical space which has zero or constant positive curvature, respectively. The negative curvature enables properties such as divergence of parallel lines and exponential volume growth with radius [3]. This volume growth property makes hyperbolic space an ideal candidate for embedding hierarchical and graph structured data [27], and has found many machine learning applications.

Lorentz Model. The Lorentz model is a way to represent a hyperbolic space. It embeds the d -dimensional hyperbolic space \mathbb{H}^d with curvature c within an $(d + 1)$ -dimensional Minkowski space $\mathbb{R}^{d,1}$, a pseudo-Euclidean space with one negative dimension, as follows:

$$\mathbb{H}^d = \{ \mathbf{x} \in \mathbb{R}^{d,1} \mid \langle \mathbf{x}, \mathbf{x} \rangle_{\mathbb{H}} = -1/c, x_0 > 0 \}, \quad (1)$$

where the Lorentzian inner product is defined as,

$$\langle \mathbf{x}, \mathbf{y} \rangle_{\mathbb{H}} = -x_0 y_0 + \sum_{i=1}^d x_i y_i. \quad (2)$$

Here, the 0-th dimension of the vector is treated as the time component and the rest as the space component. From the definition of \mathbb{H}^d , the time component can be written using the space component as follows:

$$x_{\text{time}} = x_0 = \sqrt{1/c + \|\mathbf{x}_{\text{space}}\|^2}, \quad (3)$$

where $\|\cdot\|$ is the Euclidean norm and $\mathbf{x}_{\text{space}} = \mathbf{x}_{1:d}$.

Tangent Spaces. The tangent space at a point $\mathbf{x} \in \mathbb{H}^d$ in hyperbolic space, is a Euclidean space that locally approximates hyperbolic space around \mathbf{x} . Exponential and logarithmic maps are used to project a point from a tangent space to hyperbolic space and vice versa.

3. Enforcing User-Defined Hierarchies

Our aim is to define a hierarchy in images and enforce it in the latent space using hyperbolic geometry. We first define a part-based hierarchy in images, then discuss our approach to enforce it, and finally introduce our hierarchical retrieval metric.

3.1. Part-Based Image Hierarchy

Visual hierarchies can be established in different ways, depending on the application. In this work, we are interested in a hierarchy that encapsulates the semantic relationship among objects in a scene. For this, *scene-object-part* hierarchy is appealing as it is useful for applications such as fine-grained object retrieval, object localization, and general scene understanding. This hierarchy has also been shown to emerge in hyperbolic image embeddings [21, 33].

Given an image dataset with bounding box and object class annotations, we define a part-based image hierarchy where the full scene images – typically containing multiple objects – represent the highest level in the hierarchy, while individual objects constitute progressively lower levels, *entailed* by the full image. In this, larger bounding boxes that significantly envelope smaller ones are considered to entail those smaller ones, establishing a nested hierarchy. In this way, from the full scene to the smallest bounding box, a hierarchy can be defined by recursively applying the entailment rule: *if B contained in A, then A entails B, denoted as $A \rightarrow B$* . An illustrative example is shown in Fig. 2, where an example hierarchy could be `road scene` \rightarrow `cyclist` \rightarrow `bicycle` \rightarrow `wheels`.

Pairwise Entailment. Our entailment rule above naturally facilitates a pairwise relationship. Let $I \in \mathcal{I}$ be an image, either the full scene image or a cropped bounding box, and let \mathcal{B} denote the set of all bounding boxes in the dataset. Suppose \mathcal{B}_I be the set of bounding boxes contained in the image I , i.e., $\mathcal{B}_I = \{b \in \mathcal{B} \mid b \subset I\}$ ². Note, each bounding box has an associated object label denoted by $b_l \in \mathcal{L}$.

We define the following pairwise entailment relationship:

$$\text{if } b \in \mathcal{B}_I, \text{ then } I \rightarrow b. \quad (4)$$

By applying this recursively, a tree-like hierarchy can be formed as shown in Fig. 2b. Note that our model can encode any “user-defined hierarchy” represented as entailment pairs in Eq. (4). Part-based image hierarchy is one use case.

Furthermore, if I is a full scene image, we define an additional entailment relationship across images at the object level. Specifically, for each bounding box b in the image I , we sample K bounding boxes from other images with the same label b_l and enforce entailment with the image I . Formally, let $a \in \mathcal{L}$, and let $\mathcal{B}_{I,K}^a \sim \{b \in \mathcal{B} \mid b \not\subset I, b_l = a\}$ be the set of K bounding boxes of label a on images other

²We use the \subset notation to denote *contained in* relationship. In the case where I is a cropped bounding box, this relationship is defined to hold if the majority (e.g., 80%) of the small bounding box b is contained in I .

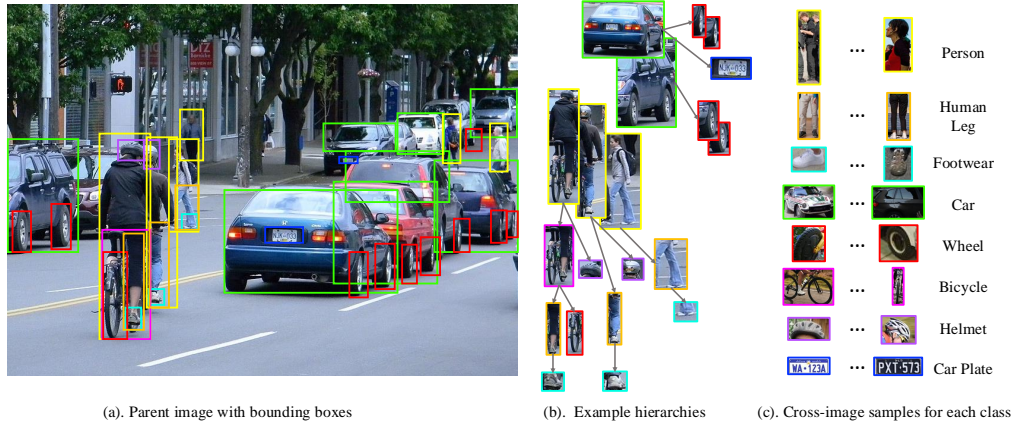


Figure 2. **An illustrative example image hierarchies.** a) Image I with object-level bounding boxes. Each bounding box is entailed by I . b) Hierarchies created via bounding box-to-bounding box entailment within I (larger bounding boxes entail smaller ones). c) Cross-image hierarchy created by sampling N bounding boxes with corresponding object classes from other images, which are then entailed by I . Find details of cross-image sampling in Sec. 3.1.

than I . We enforce the entailment as follows:

$$\text{for all } b \in \mathcal{B}_I, \text{ if } x \in \mathcal{B}_{I,K}^{b_I}, \text{ then } I \rightarrow x. \quad (5)$$

This additional entailment across images reinforces the semantic link between scenes and similar objects across different images (see Fig. 2c).

We posit that these relationships help to structure a hierarchical understanding of images based on scene, object, and part relationships.

Hierarchy Tree. As noted above, the part-based hierarchy forms a tree structure, where an image or cropped bounding box can be traversed using pairwise entailment relationships. For evaluating hierarchical image retrieval, we construct this hierarchy tree per scene/object automatically using the full training set. However, the model is trained solely on pairwise entailment relationships and does not use the hierarchy tree.

3.2. Angle-Based Entailment Loss

We require an asymmetric distance function to enforce pairwise entailment relationships in hyperbolic space. To this end, we adapt the recently proposed hyperbolic-angle-based entailment loss [33], a smooth contrastive variant of the entailment cone loss [9]. The angle-only loss, without distance con-

straints on image pairs, provides flexibility to be distributed along the radial axis, allowing embeddings to align with the tree structure while preserving pairwise entailment.

Our loss is a bidirectional version of [33], as illustrated graphically in Fig. 3. In particular, given embeddings of an entailment pair, $\mathbf{x}, \mathbf{y} \in \mathbb{R}^d$ in the tangent space, where \mathbf{x} entails \mathbf{y} , we maximize the angles β_1 and α_2 . This enforces entailment in a bidirectional manner. The angles β_1 and α_2 can be computed using the exterior angle as follows:

$$\begin{aligned} \beta_1(\mathbf{x}, \mathbf{y}) &= \pi - \text{ext}(\mathbf{x}, \mathbf{y}), \\ \alpha_2(\mathbf{y}, \mathbf{x}) &= \text{ext}(\mathbf{y}, \mathbf{x}), \end{aligned} \quad (6)$$

where $\text{ext}(\mathbf{x}, \mathbf{y})$ is the exterior angle between \mathbf{x} and \mathbf{y} and takes the following form [7]:

$$\text{ext}(\mathbf{x}, \mathbf{y}) = \cos^{-1} \left(\frac{y_{\text{time}} + x_{\text{time}} c\langle \mathbf{x}, \mathbf{y} \rangle_{\mathbb{H}}}{\|\mathbf{x}_{\text{space}}\| \sqrt{(c\langle \mathbf{x}, \mathbf{y} \rangle_{\mathbb{H}})^2 - 1}} \right). \quad (7)$$

In contrast to [33], in our case an embedding can belong to multiple entailment pairs in a batch. This corresponds to a case of multiple positives in the contrastive loss. Thus, we employ a multi-positive variant of the InfoNCE loss [29] to align all entailment pairs while pushing apart the rest of the negative pairs. Precisely, let $\mathcal{D} = \{(\mathbf{x}_i, \mathbf{y}_i)\}$ be a batch of entailment pairs. For each parent embedding \mathbf{x}_i , let \mathcal{P}_i denote the set of child embeddings

in the batch that have an entailment relationship with \mathbf{x}_i , and let \mathcal{A} denote the set of all candidate embeddings in the batch. Then the InfoNCE loss for parent-to-child can be written as:

$$L^{p \rightarrow c}(\mathcal{D}, \kappa) = -\mathbb{E}_{\mathcal{D}} \left[\log \frac{\sum_{\mathbf{y} \in \mathcal{P}_i} \exp\left(\frac{\kappa(\mathbf{x}_i, \mathbf{y})}{\tau}\right)}{\sum_{\mathbf{y} \in \mathcal{A}} \exp\left(\frac{\kappa(\mathbf{x}_i, \mathbf{y})}{\tau}\right)} \right], \quad (8)$$

where $\kappa : \mathbb{R}^d \times \mathbb{R}^d \rightarrow \mathbb{R}$ is the similarity function, and τ is a learnable temperature parameter initialized to 0.07 following [7]. Now, our bidirectional entailment loss can be written as:

$$L_{\text{angle}}(\mathcal{D}) = L^{p \rightarrow c}(\mathcal{D}, \beta_1) + L^{c \rightarrow p}(\mathcal{D}, \alpha_2). \quad (9)$$

Here, the similarity function κ is replaced with angles β_1 and α_2 so that the contrastive loss maximizes angles β_1 and α_2 for matching entailment pairs in the batch \mathcal{D} .

In our implementation, we use a shared image encoder for both parent and child embeddings. Following the reparametrization of [7], we encode the space component of the Lorentz model in the tangent space at origin and project it onto the hyperboloid using the exponential map, enabling contrastive entailment angle loss computation in hyperbolic space.

Loss in Euclidean Space. This entailment angle loss is general and can be effectively enforced in Euclidean space. In Euclidean space, the exterior angles are formulated as follows:

$$\text{ext}(\mathbf{x}, \mathbf{y})_{\mathbb{E}} = \cos^{-1} \left(\frac{\|\mathbf{y}\|^2 - \|\mathbf{x}\|^2 - \|\mathbf{x} - \mathbf{y}\|^2}{2\|\mathbf{x}\| \cdot \|\mathbf{x} - \mathbf{y}\|} \right). \quad (10)$$

Now, the loss can be analogously derived.

3.3. Hierarchical Retrieval Evaluation

To evaluate retrieval performance on the hierarchy tree, we also introduce a metric that captures the label distribution in the dataset. This is important as different labels can have different numbers of instances and the standard metrics such as Recall@k is agnostic to it.

Consider the parent-to-child relationship, and let \mathcal{H}_I denote the hierarchy tree originating from the query image I , containing m labels. Then, the labels

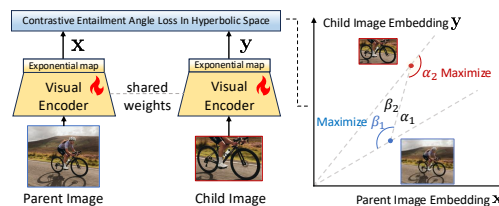


Figure 3. **Learning multi-level hierarchies via contrastive entailment angle loss.** Our model first encodes parent-to-child pairs into embeddings with exponential mapping, then maximizes β_1 and α_2 using our contrastive entailment angle loss in hyperbolic space.

in \mathcal{H}_I are the ground truth labels for the hierarchical retrieval for image I . Now, let $\mathbf{h}_I \in \mathbf{R}^m$ be the precomputed label distribution of \mathcal{H}_I . Then, our optimal transport (1-D Wasserstein) distance between the retrieved label distribution \mathbf{r}_I and \mathbf{h}_I is:

$$\text{OT}(\mathbf{h}_I, \mathbf{r}_I) = \text{Wasserstein}(\bar{\mathbf{h}}_I, \bar{\mathbf{r}}_I), \quad (11)$$

where $\bar{\cdot} \in \mathbf{R}^{m+1}$ is the label distribution with *other* class added³. Note that a smaller distance indicates better alignment.

4. Related Work

Hyperbolic geometry allows for exponential volume growth with respect to the radius [3], making it effective for embedding hierarchical structures. This advantage has led to significant research into leveraging hyperbolic representations for various data types, including molecular structures [42], 3D [4, 18, 40], images [12, 13, 21, 22, 31], text data [10, 19, 38, 38, 43], and vision-language data [2, 7, 23, 33].

Hyperbolic embeddings can be learned through standard deep learning layers [20] with hyperbolic projection [27] or using hyperbolic neural networks [10]. Many prior NLP, computer vision and knowledge graph studies learn hierarchies from partially order data [10, 25, 39], or minimizing geodesic distance or maximizing similarities [12, 27, 28, 41]. Ganea et al. [10] introduced an angle-based entailment cone loss which pushes child nodes into the cone emanating from the par-

³For \mathbf{h}_I other class has zero mass, and for \mathbf{r}_I all labels not in \mathcal{H}_I are combined to form the other class.

ent node embedding. This approach has been applied to both text [10] and image data [8] with label hierarchies. Recently, this hyperbolic entailment loss was adapted for contrastive learning to develop representations in vision-language models [2, 7, 30, 33]. However, such methods remain relatively unexplored in the image domain. We adapted the angle-based entailment loss from [33] to encode part-based image hierarchies. Many previous works are limited to learning hierarchies for single-class images using predefined labeled hierarchies, such as ImageNet [21, 26] or hand-labeled data [8]. In this work, we propose a learning method that fine-tunes pre-trained models on large-scale datasets for **general images** (with multiple classes per image) **without hierarchical labels**. The most relevant approach, HCL [12], models simple scene-to-object hierarchies, whereas we capture more complex, multi-level part-based hierarchies directly from image data, extending beyond visual similarity.

5. Experiments

Datasets. For training and evaluation, we construct *HierOpenImages*, a novel dataset containing pairwise part-based image hierarchies built from the OpenImages dataset [24]. We further evaluate generalization on out-of-domain datasets and hierarchies.

Models. We evaluate the performance of learning multi-level image hierarchies using two popular visual encoders 1) CLIP ViT (B/16) [32], pretrained on large-scale image-text pairs from the Internet, and 2) MoCo-v2 (ResNet-50) [6], pretrained on ImageNet. Note that both CLIP and MoCo-v2 models are fine-tuned and evaluated in an **image encoder only** setting. We use these pretrained image models as our baseline and compare our proposed angle-based hyperbolic method against its Euclidean counterpart. Each model is fine-tuned on *HierOpenImages* using the proposed contrastive angle-based entailment loss, and † denotes fine-tuning. Note that * denotes the gated entailment angle metric, which first uses the entailment angle as a cone-shaped filter and then applies the pretrained metric within the gated set for fine-grained ranking (see Supp. §B.2).

We compare the state-of-the-art hyperbolic hierarchical image-only model HCL [12], which is

trained on scene-to-object relationships from the OpenImages dataset [24] in both hyperbolic and Euclidean space. Accordingly, we evaluate the retrieval performance of HCL [12] using both hyperbolic distance and cosine similarity. For completeness, we also fine-tuned HCL† [12] on the *HierOpenImages* dataset. Note that fine-tuning or evaluating with a text encoder is not possible on the *HierOpenImages* dataset. Furthermore, previous image-only supervised methods, trained on predefined single-class image hierarchies [8, 21] are not directly comparable. These methods require all image classes to be predefined during training, which is not feasible for complex multi-object scenes in the OpenImages [24] and LVIS [14] datasets, where images contain multiple objects with diverse class labels.⁴

5.1. Main Results

In same-class retrieval, we assess whether the retrieved image belongs to the *same class* as the query image. In hierarchical retrieval, we verify if the retrieved image exists within the *hierarchy tree* of the query image, specifically evaluating the quality of the learned hierarchical representations.

Same-Class Retrieval. Denoting the full image as *parent* and the bounding box as *child*, we evaluate retrieval tasks in both child-to-parent and parent-to-child directions. Table 1 shows the retrieval accuracy of top-k = {5, 10, 50, 100}. We notice a consistent improvement with our proposed hyperbolic model, across all metrics and model variants. This highlights the relevance of our angle-based entailment loss and the advantages of learning hierarchical image embeddings in hyperbolic space.

Hierarchical Retrieval via the Learned Latent Space Distribution. Table 2 evaluates the hierarchical structure of the latent space by retrieving a large number of child images from parent images. We use recall to measure the percentage of ground truth images that are successfully retrieved. Moreover, we check the alignment between the retrieved

⁴Updated results after fixing an extra normalization issue in the code which impacted the results of all methods; overall trends and conclusions remain unaffected.

Vision Encoder	Model	Metrics	Top-5	Top-10	Top-50	Top-100
Child-to-Parent						
CLIP ViT	CLIP	Cos Sim.	53.04	51.69	47.87	45.79
	CLIP-euc [†]	Euc Ang.*	75.63	74.65	72.25	70.52
	CLIP-hyp [†]	Hyp Ang.*	77.28	75.91	72.85	70.94
MoCo-v2	HCL	Hyp Dist.	46.57	44.86	39.64	36.61
	HCL	Cos Sim.	55.48	54.81	52.23	50.67
	HCL [†]	Hyp Dist.	39.71	37.55	32.13	29.44
	HCL [†]	Cos Sim.	56.76	55.85	53.61	52.16
	MoCo	Cos Sim.	53.72	52.71	50.41	49.19
	MoCo-euc [†]	Euc Ang.*	66.78	66.58	65.42	64.40
	MoCo-hyp [†]	Hyp Ang.*	68.62	67.42	66.21	64.94
	MoCo-hyp [†]	Hyp Ang.*	68.62	67.42	66.21	64.94
Parent-to-Child						
CLIP ViT	CLIP	Cos Sim.	69.94	67.74	62.50	60.21
	CLIP-euc [†]	Euc Ang.*	73.74	72.57	70.04	68.78
	CLIP-hyp [†]	Hyp Ang.*	74.48	73.27	70.78	69.46
MoCo-v2	HCL	Hyp Dist.	50.86	49.81	47.34	46.06
	HCL	Cos Sim.	53.64	53.04	51.34	50.59
	HCL [†]	Hyp Dist.	53.29	52.39	50.04	48.74
	HCL [†]	Cos Sim.	54.99	54.36	52.86	52.03
	MoCo	Cos Sim.	63.65	62.21	58.85	57.28
	MoCo-euc [†]	Euc Ang.*	68.87	67.94	65.64	64.42
	MoCo-hyp [†]	Hyp Ang.*	69.50	68.14	65.67	64.46
	MoCo-hyp [†]	Hyp Ang.*	69.50	68.14	65.67	64.46

Table 1. **Part-based same-class image retrieval evaluation.** For child-to-parent image retrieval, the retrieved parent must contain the object class of the query child. For parent-to-child image retrieval, the retrieved child must match a class within the parent. [†] denotes models fine-tuned on the *HierOpenImages* dataset. Our proposed method is shaded in purple.

Metrics	Model	Dist. Func.	Top-150k	Top-200k	Top-250k
CLIP ViT					
Recall \uparrow	CLIP	Cos Sim.	66.63	77.15	86.57
	CLIP-euc [†]	Euc Ang.*	76.46	85.08	91.38
	CLIP-hyp [†]	Hyp Ang.*	77.00	85.75	91.89
OT Distance \downarrow	CLIP	Cos Sim.	21.31	22.74	23.79
	CLIP-euc [†]	Euc Ang.*	15.65	18.15	21.09
	CLIP-hyp [†]	Hyp Ang.*	14.96	17.57	20.76
MoCo-v2					
Recall \uparrow	HCL	Hyp Dist.	51.83	64.84	77.66
	HCL	Cos Sim.	57.05	67.65	78.71
	HCL [†]	Hyp Dist.	54.51	66.70	78.83
	HCL [†]	Cos Sim.	60.13	70.26	80.51
	MoCo	Cos Sim.	65.01	75.85	85.61
	MoCo-euc [†]	Euc Ang.*	74.84	83.71	90.46
MoCo-hyp [†]	Hyp Ang.*	74.85	83.79	90.61	
OT Distance \downarrow	HCL	Hyp Dist.	24.58	24.84	25.01
	HCL	Cos Sim.	23.58	24.65	25.11
	HCL [†]	Hyp Dist.	25.30	25.63	25.53
	HCL [†]	Cos Sim.	21.94	23.58	24.58
	MoCo	Cos Sim.	18.60	20.79	22.56
	MoCo-euc [†]	Euc Ang.*	16.65	18.75	21.38
MoCo-hyp [†]	Hyp Ang.*	16.59	18.65	21.29	

Table 2. **Part-based hierarchical evaluation of parent-to-child image retrieval on *HierOpenImages*.** Results are evaluated using the ground truth hierarchy tree and the hierarchical distribution of the test set. Smaller OT distance indicates better distribution alignment.

distribution and the underlying hierarchical distribution of the full test set. Good distribution alignment is a desirable property for fine-grained retrieval as the *retrieved set should capture the hierarchies present in the data distribution*. We propose to measure distribution alignment using the optimal trans-

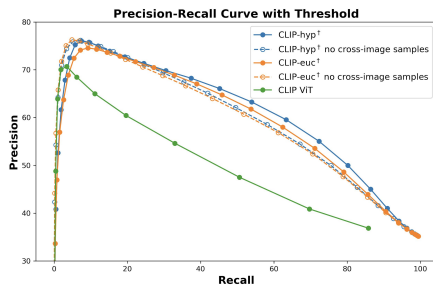


Figure 4. **Precision-Recall curves of CLIP ViT models on hierarchical retrieval.** Dotted lines show models trained only on hierarchical entailment data within the same images; solid lines represent models trained with additional cross-image scene-to-object samples.

port (Wasserstein distance), with a smaller distance indicating a closer match (see Sec. 3.3).

As shown in Table 2, our hyperbolic model better captures the hierarchical distribution of the test set compared to the Euclidean model, achieving better recall and OT distance in all cases. All fine-tuned models using our angle-based entailment loss show clear improvement over the baseline models. In contrast, HCL [12] shows only a small gain after fine-tuning, suggesting that its training method is not well suited for capturing the complex visual hierarchies in our data.

Effect of Enforcing Cross Image Entailment. To compare the emergent behaviors of the hyperbolic and Euclidean models, we trained the CLIP ViT model solely on hierarchical part-based entailment data within individual images (entailment pairs with high visual similarity), omitting any cross-image image-to-bounding-box samples.

Fig. 4 shows the Precision-Recall (PR) curve with increasing β_1 angle thresholds (0 to π) for CLIP-hyp[†] and CLIP-euc[†], and with cosine similarity thresholds (0 to 1) for the baseline CLIP. Fine-tuning in both Euclidean and Hyperbolic spaces substantially improves performance from the pretrained model. Introducing cross-image pairs further improves recall in the mid-to-high recall regions, indicating better alignment across semantically related but visually diverse examples, with only a small precision drop at the top ranks due to the added variability from cross-image relationships.

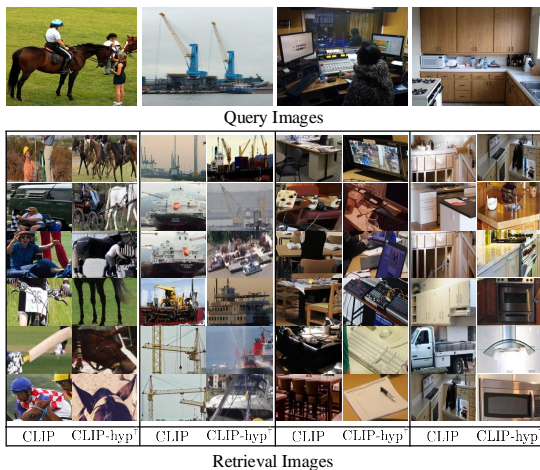


Figure 5. **Example of parent-to-child retrieval using CLIP ViT and our CLIP-hyp[†] model.** Results are ordered by ascending norms. Our model retrieves images matching the predefined *scene-object-part* hierarchy, placing high-level objects near the origin (e.g., harbor → boat parts), and grouping semantically related but visually distinct objects (e.g., microwave oven & kitchen hood).

Qualitative Results. Following [7, 11, 33], we use parent-to-child image traversals with results ordered by increasing embedding norm, to illustrate the latent space, which: (1) aligns with the predefined *scene-object-part* hierarchy, placing high-level objects near the origin. (2). groups diverse objects under the same lower hierarchical branch, even if they are visually distinct (e.g., keyboard and monitor under the studio image). Moreover, Figure 10 shows an example of the model’s emergent structure where high-frequency, ambiguous image crops are naturally pushed toward the boundary of hyperbolic space. Find details in supplementary materials.

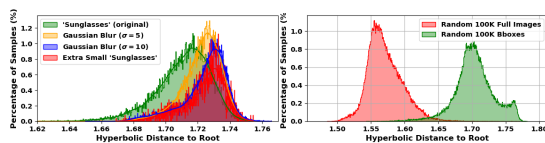


Figure 6. **Example of the model’s emergent structure.**

5.2. Generalization Evaluation

We evaluate the generalization of our method through image retrieval on unseen datasets and hi-

Model	Dist. Func.	Top-5	Top-10	Top-50	Top-100
Child-to-Parent					
CLIP	Cos Sim.	15.00	14.22	11.91	10.48
CLIP-euc [†]	Euc Ang.*	28.45	26.76	22.65	20.43
CLIP-hyp [†]	Hyp Ang.*	28.84	27.02	22.87	20.53
Parent-to-Child					
CLIP	Cos Sim.	28.37	27.35	24.99	23.36
CLIP-euc [†]	Euc Ang.*	28.84	27.02	22.65	20.43
CLIP-hyp [†]	Hyp Ang.*	30.27	29.53	27.83	26.81

Metrics	Model	Dist. Func.	Top-10k	Top-20k	Top-30k
Recall ↑	CLIP	Cos Sim.	42.40	57.22	67.98
	CLIP-euc [†]	Euc Ang.*	53.54	68.77	78.61
	CLIP-hyp [†]	Hyp Ang.*	53.87	69.13	78.85
OT Distance ↓	CLIP	Cos Sim.	6.25	7.89	8.76
	CLIP-euc [†]	Euc Ang.*	5.49	7.04	8.05
	CLIP-hyp [†]	Hyp Ang.*	5.56	7.13	8.13

Table 3. **Out-of-domain part-based image retrieval evaluation on the LVIS dataset:** same-class (top) and part-based hierarchical retrieval (bottom).

Dataset	CLIP	CLIP-euc [†]	CLIP-hyp [†]
VOC	87.3	93.6	94.2
COCO	63.6	73.4	73.9

Table 4. **Zero-shot object detection using ground-truth boxes.** Image-only model with top-5 majority voting.

erarchies. Similar to Table 1-2, Table 3 presents part-based same-class and hierarchical retrieval performance on the **out-of-domain** LVIS dataset [14], which contains 1,203 fine-grained object classes, including many rare objects absent from the training *HierOpenImages* dataset. Table 4 evaluates image retrieval performance on VOC and COCO datasets following the zero-shot object detection in [30] where ground-truth boxes are used as region proposals, and then predict via top-5 majority vote. Results demonstrate that our visual hierarchical learning significantly enhances model generalization on unseen datasets and image hierarchies.

6. Conclusion

In this work, we introduce a new learning paradigm that effectively encodes user-defined visual hierarchies in hyperbolic space without requiring explicit hierarchical labels. We present a concrete example of defining a part-based multi-level complex image hierarchy using object-level annotations and propose a contrastive loss in hyperbolic space to enforce pairwise entailment relationships. Additionally, we introduce new evaluation metrics for hierarchical image retrieval. Our experiments demonstrate our model effectively learns the predefined image hierarchy and goes beyond visual similarity.

References

- [1] Abubakar Abid, Ali Abdalla, Ali Abid, Dawood Khan, Abdulrahman Alfozan, and James Zou. Gradio: Hassle-free sharing and testing of ml models in the wild. *arXiv preprint arXiv:1906.02569*, 2019. 15
- [2] Morris Alper and Hadar Averbuch-Elor. Emergent visual-semantic hierarchies in image-text representations. In *Proceedings of the European Conference on Computer Vision (ECCV)*, 2024. 5, 6
- [3] Martin R Bridson and André Haeffliger. *Metric spaces of non-positive curvature*. Springer Science & Business Media, 2013. 2, 5
- [4] Jiaxin Chen, Jie Qin, Yuming Shen, Li Liu, Fan Zhu, and Ling Shao. Learning attentive and hierarchical representations for 3d shape recognition. In *Computer Vision—ECCV 2020: 16th European Conference, Glasgow, UK, August 23–28, 2020, Proceedings, Part XV 16*, pages 105–122. Springer, 2020. 5
- [5] Ting Chen, Simon Kornblith, Mohammad Norouzi, and Geoffrey Hinton. A simple framework for contrastive learning of visual representations. In *International conference on machine learning*, pages 1597–1607. PMLR, 2020. 1
- [6] Xinlei Chen, Haoqi Fan, Ross Girshick, and Kaiming He. Improved baselines with momentum contrastive learning. *arXiv preprint arXiv:2003.04297*, 2020. 6
- [7] Karan Desai, Maximilian Nickel, Tanmay Rajpurohit, Justin Johnson, and Shanmukha Ramakrishna Vedantam. Hyperbolic image-text representations. In *International Conference on Machine Learning*, pages 7694–7731. PMLR, 2023. 2, 4, 5, 6, 8
- [8] Ankit Dhall, Anastasia Makarova, Octavian Ganea, Dario Pavlo, Michael Greeff, and Andreas Krause. Hierarchical image classification using entailment cone embeddings. In *Proceedings of the IEEE/CVF conference on computer vision and pattern recognition workshops*, pages 836–837, 2020. 6
- [9] Octavian Ganea, Gary Bécigneul, and Thomas Hofmann. Hyperbolic entailment cones for learning hierarchical embeddings. In *International Conference on Machine Learning*, pages 1646–1655. PMLR, 2018. 4
- [10] Octavian Ganea, Gary Bécigneul, and Thomas Hofmann. Hyperbolic neural networks. *Advances in neural information processing systems*, 31, 2018. 5, 6
- [11] Songwei Ge, Shlok Kumar Mishra, Haohan Wang, Chun-Liang Li, and David Jacobs. Robust contrastive learning using negative samples with diminished semantics. In *NeurIPS*, 2021. 8
- [12] Songwei Ge, Shlok Mishra, Simon Kornblith, Chun-Liang Li, and David Jacobs. Hyperbolic contrastive learning for visual representations beyond objects. In *Proceedings of the IEEE/CVF Conference on Computer Vision and Pattern Recognition*, pages 6840–6849, 2023. 2, 5, 6, 7
- [13] Yunhui Guo, Xudong Wang, Yubei Chen, and Stella X Yu. Clipped hyperbolic classifiers are super-hyperbolic classifiers. In *Proceedings of the IEEE/CVF Conference on Computer Vision and Pattern Recognition*, pages 11–20, 2022. 5
- [14] Agrim Gupta, Piotr Dollar, and Ross Girshick. Lvis: A dataset for large vocabulary instance segmentation. In *Proceedings of the IEEE/CVF conference on computer vision and pattern recognition*, pages 5356–5364, 2019. 6, 8, 16
- [15] Kaiming He, Xiangyu Zhang, Shaoqing Ren, and Jian Sun. Deep residual learning for image recognition. In *Proceedings of the IEEE conference on computer vision and pattern recognition*, pages 770–778, 2016. 1
- [16] Kaiming He, Haoqi Fan, Yuxin Wu, Saining Xie, and Ross Girshick. Momentum contrast for unsupervised visual representation learning. In *CVPR*, 2020.
- [17] Elad Hoffer and Nir Ailon. Deep metric learning using triplet network. In *Similarity-based pattern recognition: third international workshop, SIMBAD 2015, Copenhagen, Denmark, October 12-14, 2015. Proceedings 3*, pages 84–92. Springer, 2015. 1
- [18] Joy Hsu, Jeffrey Gu, Gong Wu, Wah Chiu, and Serena Yeung. Capturing implicit hierarchical structure in 3d biomedical images with self-supervised hyperbolic representations. *Advances in neural information processing systems*, 34:5112–5123, 2021. 5
- [19] Yoo Hyun Jeong, Myeongsoo Han, and Dong-Kyu Chae. A simple angle-based approach for contrastive learning of unsupervised sentence representation. In *Findings of the Association for Computational Linguistics: EMNLP 2024*, pages 5553–5572, 2024. 5
- [20] Salman Khan, Muzammal Naseer, Munawar Hayat, Syed Waqas Zamir, Fahad Shahbaz Khan, and Mubarak Shah. Transformers in vision: A sur-

- vey. *ACM computing surveys (CSUR)*, 54(10s):1–41, 2022. 5
- [21] Valentin Khrulkov, Leyla Mirvakhabova, Evgeniya Ustinova, Ivan Oseledets, and Victor Lempitsky. Hyperbolic image embeddings. In *Proceedings of the IEEE/CVF Conference on Computer Vision and Pattern Recognition*, pages 6418–6428, 2020. 2, 3, 5, 6
- [22] Sungyeon Kim, Boseung Jeong, and Suha Kwak. Hier: Metric learning beyond class labels via hierarchical regularization. In *Proceedings of the IEEE/CVF Conference on Computer Vision and Pattern Recognition*, pages 19903–19912, 2023. 5
- [23] Fanjie Kong, Yanbei Chen, Jiarui Cai, and Davide Modolo. Hyperbolic learning with synthetic captions for open-world detection. In *Proceedings of the IEEE/CVF Conference on Computer Vision and Pattern Recognition*, pages 16762–16771, 2024. 5
- [24] Alina Kuznetsova, Hassan Rom, Neil Alldrin, Jasper Uijlings, Ivan Krasin, Jordi Pont-Tuset, Shahab Kamali, Stefan Popov, Matteo Mallocci, Alexander Kolesnikov, et al. The open images dataset v4: Unified image classification, object detection, and visual relationship detection at scale. *International journal of computer vision*, 128(7):1956–1981, 2020. 2, 6, 12, 16
- [25] Qi Liu, Maximilian Nickel, and Douwe Kiela. Hyperbolic graph neural networks. *NeurIPS*, 2019. 5
- [26] Shaoteng Liu, Jingjing Chen, Liangming Pan, Chong-Wah Ngo, Tat-Seng Chua, and Yu-Gang Jiang. Hyperbolic visual embedding learning for zero-shot recognition. In *CVPR*, 2020. 6
- [27] Maximilian Nickel and Douwe Kiela. Poincaré embeddings for learning hierarchical representations. *Advances in neural information processing systems*, 30, 2017. 1, 2, 5
- [28] Maximilian Nickel and Douwe Kiela. Learning continuous hierarchies in the lorentz model of hyperbolic geometry. In *International conference on machine learning*, pages 3779–3788. PMLR, 2018. 2, 5
- [29] Aaron van den Oord, Yazhe Li, and Oriol Vinyals. Representation learning with contrastive predictive coding. *arXiv preprint arXiv:1807.03748*, 2018. 4
- [30] Avik Pal, Max van Spengler, Guido Maria D’Amely di Melendugno, Alessandro Flaborea, Fabio Galasso, and Pascal Mettes. Compositional entailment learning for hyperbolic vision-language models. *arXiv preprint arXiv:2410.06912*, 2024. 6, 8
- [31] Zexuan Qiu, Jiahong Liu, Yankai Chen, and Irwin King. Hihpq: Hierarchical hyperbolic product quantization for unsupervised image retrieval. In *Proceedings of the AAAI Conference on Artificial Intelligence*, pages 4614–4622, 2024. 2, 5
- [32] Alec Radford, Jong Wook Kim, Chris Hallacy, Aditya Ramesh, Gabriel Goh, Sandhini Agarwal, Girish Sastry, Amanda Askell, Pamela Mishkin, Jack Clark, et al. Learning transferable visual models from natural language supervision. In *International conference on machine learning*, pages 8748–8763. PMLR, 2021. 6
- [33] Sameera Ramasinghe, Violetta Shevchenko, Gil Avraham, and Ajanthan Thalaiyasingam. Accept the modality gap: An exploration in the hyperbolic space. In *Proceedings of the IEEE/CVF Conference on Computer Vision and Pattern Recognition*, pages 27263–27272, 2024. 2, 3, 4, 5, 6, 8
- [34] John G Ratcliffe, S Axler, and KA Ribet. *Foundations of hyperbolic manifolds*. Springer, 1994. 2
- [35] Erzsébet Ravasz and Albert-László Barabási. Hierarchical organization in complex networks. *Physical review E*, 67(2):026112, 2003. 1
- [36] Frederic Sala, Chris De Sa, Albert Gu, and Christopher Ré. Representation tradeoffs for hyperbolic embeddings. In *ICML*, 2018. 2
- [37] Florian Schroff, Dmitry Kalenichenko, and James Philbin. Facenet: A unified embedding for face recognition and clustering. In *Proceedings of the IEEE conference on computer vision and pattern recognition*, pages 815–823, 2015. 1
- [38] Alexandru Tifrea, Gary Bécigneul, and Octavian-Eugen Ganea. Poincaré glove: Hyperbolic word embeddings. *arXiv preprint arXiv:1810.06546*, 2018. 5
- [39] Luke Vilnis, Xiang Li, Shikhar Murty, and Andrew McCallum. Probabilistic embedding of knowledge graphs with box lattice measures. *arXiv preprint arXiv:1805.06627*, 2018. 5
- [40] Sijie Wang, Qiyu Kang, Rui She, Wei Wang, Kai Zhao, Yang Song, and Wee Peng Tay. Hypliloc: Towards effective lidar pose regression with hyperbolic fusion. In *Proceedings of the IEEE/CVF Conference on Computer Vision and Pattern Recognition*, pages 5176–5185, 2023. 5
- [41] Jiexi Yan, Lei Luo, Cheng Deng, and Heng Huang. Unsupervised hyperbolic metric learning. In *CVPR*, 2021. 5

- [42] Zhen Yu, Toan Nguyen, Yaniv Gal, Lie Ju, Shekhar S Chandra, Lei Zhang, Paul Bonnington, Victoria Mar, Zhiyong Wang, and Zongyuan Ge. Skin lesion recognition with class-hierarchy regularized hyperbolic embeddings. In *International Conference on Medical Image Computing and Computer-Assisted Intervention*, pages 594–603. Springer, 2022. [5](#)
- [43] Yudong Zhu, Di Zhou, Jinghui Xiao, Xin Jiang, Xiao Chen, and Qun Liu. Hypertext: Endowing fasttext with hyperbolic geometry. *arXiv preprint arXiv:2010.16143*, 2020. [5](#)

APPENDICES

A. Hierarchy Tree

Our part-based image hierarchy framework is designed to be widely applicable to general image datasets with bounding box annotations. In this section, we outline the key implementation involved in constructing hierarchy trees.

We introduce a general method to generate dataset-specific ground truth hierarchy trees based on data statistics. Following the approach outlined in Sec. 3.1 of the main paper, we begin by identifying bounding box pairs with substantial overlap. In this work, we define a bounding box pair when at least 80% of the smaller bounding box b is contained within either the full image or a larger bounding box. We initially set the overlap threshold at 100% and empirically adjusted it by evaluating the hierarchy’s validity using text labels. For the OpenImages dataset, 80% was found to be a suitable threshold. This is a design choice and can be adapted for other datasets.

These pairs are then filtered based on two criteria: a *frequency* threshold and a *proportion* threshold. For each pair, we record the *frequency* of occurrences (e.g., bicycle-to-wheel relationships) and calculate the *proportion* of instances where a child class appears within a parent class (e.g., the percentage of bicycle bounding boxes containing a wheel bounding box). Only pairs meeting both criteria, frequent occurrence and consistent labeling, are preserved. We choose *frequency* = 50 and *proportion* = 10% in our experiments.

Once entailment pairs are established, they are organized into hierarchical trees (see examples in Fig. 7). In the evaluation of hierarchical image retrieval, the order of the hierarchy tree is essential: for parent-to-child retrieval, lower-level concepts below the child in the hierarchy tree are considered correct, while for child-to-parent retrieval, higher-level concepts above the input classes are correct.

B. Experiment Details

B.1. Hyperparameters and training details

We employ the AdamW optimizer with parameters $(\beta_1, \beta_2) = (0.9, 0.999)$ and a learning rate of 2×10^{-5} . Training was conducted using $8 \times A10G$ Nvidia GPUs. For each model, we used the largest batch size that fit in memory: CLIP ViT was trained with a total effective batch size of 640, and MoCo-v2 with a total effective batch size of 1984. Each model was fine-tuned on *HierOpenImages* dataset. The embeddings are projected to dimension 128 in the final layer. The hyperbolic model has a learnable curvature parameter.

During training, we filter out bounding boxes that occupy less than 1% of the full image area, as well as pairs involving small bounding boxes labeled as ‘IsGroupOf’ objects in the bounding box-to-bounding box relationships. For data augmentation, we apply randomly horizontal flip (20%), vertical flip(20%), rotate (degree =15), color jitter (brightness=0.2, contrast=0.2, saturation=0.2, hue=0.1), Gaussian blur (kernel size=5, $\sigma = (0.3, 1.5)$), and then resize each image to 224×224 .

B.2. Part-based Image Retrieval

Data. *HierOpenImages* is built from the OpenImages dataset [24], which originally contains approximately 1.9 million images, 14 million bounding boxes and 600 labels. We create image-to-bounding box pairs, including one cross-image bounding box sample for each bounding box class in the image, and bounding box to bounding box pairs where at least 80% of the smaller bounding box is contained in the larger bounding box.

During part-based image retrieval evaluation, we filter out bounding boxes for very small or large objects, and filter out noisy samples (e.g., wrong labels, highly occluded, etc). For part-based image retrieval, we randomly select a subset of 10,000 full images and 10,000 bounding box images as query images, using the entire filtered test set as candidates. The top-50 class frequency distributions for both the query and candidate sets are shown in Fig. 8. Although the query and candidate set distributions are similar, the class distribution is highly imbalanced,

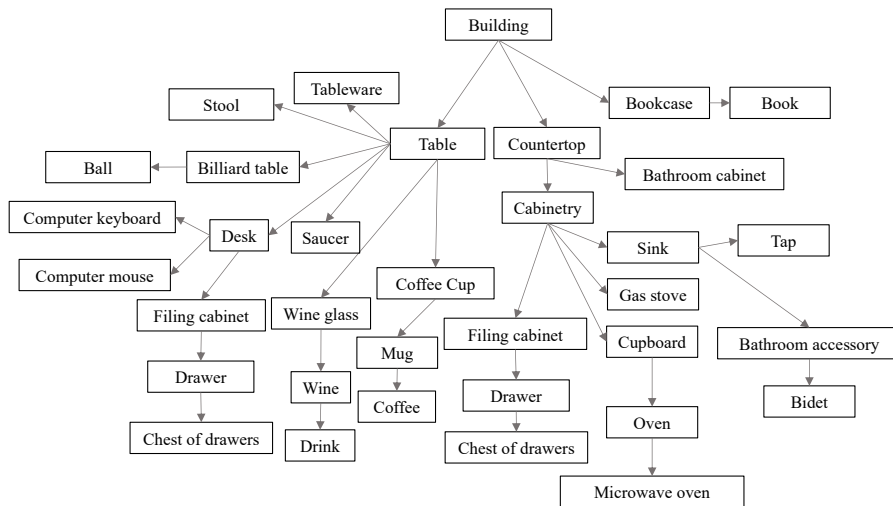


Figure 7. Example of a subset of hierarchical trees extracted from the OpenImages dataset.

highlighting the importance of hierarchical retrieval evaluation using combined precision-recall curves and OT distances (Sec. 3.3; see Fig. 4 and Table 2 in the main paper).

Gated Entailment Angle Metric. In this work, all entailment-angle thresholds are measured in radians. We use a threshold of 2 for MoCo and 2.5 for CLIP in small-k same-class classification, and a threshold of 1 for both models in large-k hierarchical retrieval.

Same-Class Retrieval. For part-to-full retrieval, a retrieval is considered correct if the retrieved full image contains the same object class as the query bounding box image. For full-to-part retrieval, a retrieval is correct if the retrieved bounding box image corresponds to an object class within the query full image.

Hierarchical Retrieval. From a query parent image, correct child classes are all classes located at the lower level on the hierarchy tree of the labeled classes of the parent image (see examples in Fig. 7). For instance, when querying with a high-level full

image, such as an image of a car, we expect to retrieve lower-level bounding boxes associated with the car, such as the car mirror, wheel or car plate *etc.* Conversely, when querying with a bounding box image, such as a wheel, we expect to retrieve various types of higher-level full images that include wheels, like cars, bicycles or cyclists *etc.*

Hierarchical Retrieval Evaluation To compute the optimal transport (1-D Wasserstein) distance between the retrieved label distribution and the ground truth (Table 2 and Fig. 4 in the main paper), we construct the ground truth distribution based on the frequency of each class (and its hierarchical classes) in the query parent image. We count the occurrences of each class in the candidate set and build the ground truth distribution by normalizing the frequencies to sum to 1. Similarly, the retrieval distribution is built by counting and normalizing retrieved class occurrences, and assigning any retrieved classes outside the ground truth hierarchy to an ‘others’ class. The two distributions are aligned by class order (ground truth distribution is zero in the ‘others’ class), and the 1-D Wasserstein distance is computed using the `scipy` library.

Note that the Wasserstein distance has a closed-

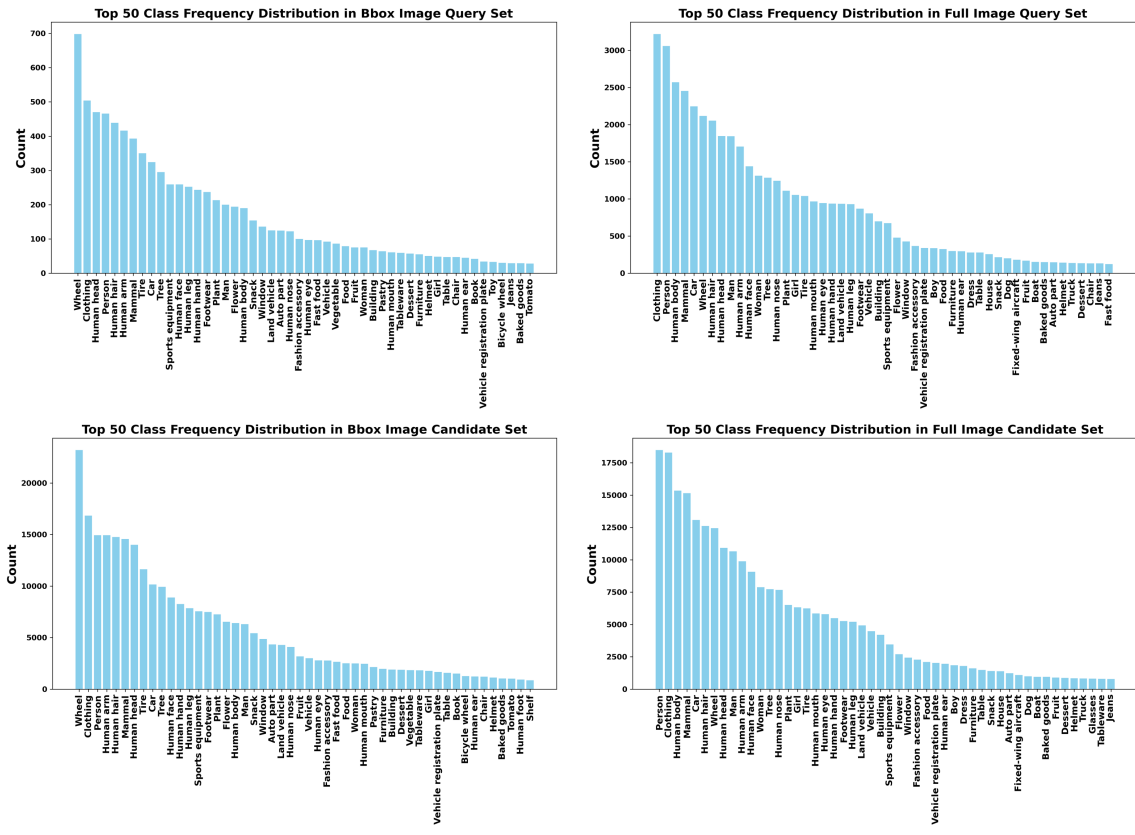


Figure 8. Bounding box class distribution in the candidate and query sets.

form formula for 1-D data. If P and Q are represented as discrete empirical distributions (e.g., histograms or sorted samples of size n), let $\{x_1, x_2, \dots, x_n\}$ to be sorted values P , and $\{y_1, y_2, \dots, y_n\}$ to be sorted values from Q , then the 1-D Wasserstein distance is:

$$W_p(P, Q) = \left(\frac{1}{n} \sum_{i=1}^n \|x_i - y_i\|^p \right)^{1/p},$$

where p refers to the order of the distance in the general p-Wasserstein metric.

In Table 2 of the main paper, we retrieve the Top-K results starting from a large K. This is necessary because each image contains an average of 5.29 distinct classes and 61.5 classes across hierarchical trees, requiring a large number of retrievals

to accurately evaluate the distribution.

Gated Entailment Angle Metric. In Table 5, we report retrieval performance using three metrics for completeness: cosine similarity (the model’s pretrained metric), entailment angle (the finetuned metric), and a gated entailment angle metric (Ang.*), which combines the strengths of both.

The gated approach first uses the entailment angle as a cone-shaped filter to retain only candidates that satisfy the desired hierarchical direction (e.g., retrieving a parent or child image) and discards those that violate the entailment relationship. Cosine similarity is then applied within this gated set to provide fine-grained ranking. This two-stage procedure ensures that retrieval respects semantic hierar-

Vision Encoder	Model	Metrics	Top-5	Top-10	Top-50	Top-100
Child-to-Parent						
CLIP ViT	CLIP-euc [†]	Cos Sim.	75.20	74.32	71.81	70.21
	CLIP-hyp [†]	Cos Sim.	76.82	75.53	72.46	70.50
	CLIP-euc [†]	Euc Ang.	75.35	74.23	72.45	70.78
	CLIP-hyp [†]	Hyp Ang.	76.95	75.97	72.94	71.04
	CLIP-euc [†]	Euc Ang.*	75.63	74.65	72.25	70.52
	CLIP-hyp [†]	Hyp Ang.*	77.28	75.91	72.85	70.94
MoCo-v2	MoCo-euc [†]	Cos Sim.	67.93	67.67	66.20	65.04
	MoCo-hyp [†]	Cos Sim.	69.00	68.37	66.26	64.96
	MoCo-euc [†]	Euc Ang.	47.00	46.64	43.36	41.00
	MoCo-hyp [†]	Hyp Ang.	49.91	48.93	43.73	40.95
	MoCo-euc [†]	Euc Ang.*	66.78	66.58	65.42	64.40
	MoCo-hyp [†]	Hyp Ang.*	68.62	67.42	66.21	64.94
Parent-to-Child						
CLIP ViT	CLIP-euc [†]	Cos Sim.	73.73	72.52	69.97	68.70
	CLIP-hyp [†]	Cos Sim.	74.38	73.20	70.67	69.28
	CLIP-euc [†]	Euc Ang.	72.59	71.58	69.49	68.46
	CLIP-hyp [†]	Hyp Ang.	73.80	72.89	70.67	69.52
	CLIP-euc [†]	Euc Ang.*	73.74	72.57	70.04	68.78
	CLIP-hyp [†]	Hyp Ang.*	74.48	73.27	70.78	69.46
MoCo-v2	MoCo-euc [†]	Cos Sim.	66.68	65.90	64.20	63.25
	MoCo-hyp [†]	Cos Sim.	66.80	65.88	64.07	63.11
	MoCo-euc [†]	Euc Ang.	67.21	66.23	63.47	61.85
	MoCo-hyp [†]	Hyp Ang.	67.53	66.14	62.50	60.82
	MoCo-euc [†]	Euc Ang.*	68.87	67.94	65.64	64.42
	MoCo-hyp [†]	Hyp Ang.*	69.50	68.14	65.67	64.46

Table 5. **Part-based same-class image retrieval evaluation using different metrics.** Cosine similarity (Cos Sim.) is the pretrained metric, entailment angle (Euc or Hyp Ang.) is the finetuned metric, and * represents a gated entailment angle metric which combines the strengths of both.

embedding norms. Additional functionalities can be easily integrated into the current pipeline.

B.3. Generalization Evaluation

LVIS Dataset. We evaluate the generalization capability of our model on the out-of-domain LVIS dataset [14], which is designed for large-scale (~1.2M bounding boxes) long-tail instance classification and segmentation. It has a highly imbalanced distribution of 1,203 object categories and contains 897 object categories that are absent from OpenImages [24]. Here are some examples of unseen hierarchies in LVIS [14] but not in OpenImages [24]: {table → tablecloth → ashtray → cigarette}, {backpack → strap → belt buckle}, {toy → teddy bear → thread → bobbin}, {sofa → blanket → quilt → bedspread}. The full list of these categories can be found in the appendix. Only display the first class of synonyms.

We construct the hierarchical evaluation set from

Model	Cross-Image	Top-5	Top-10	Top-50	Top-100
Child-to-Parent					
CLIP-hyp [†]	✓	77.28	75.91	72.85	70.94
CLIP-euc [†]	✓	75.63	74.65	72.25	70.52
CLIP-hyp [†]	✗	73.56	71.57	68.25	66.60
CLIP-euc [†]	✗	73.32	71.26	67.33	65.67
CLIP	-	53.04	51.69	47.87	45.79
Parent-to-Child					
CLIP-hyp [†]	✓	74.48	73.27	70.78	69.46
CLIP-euc [†]	✓	73.74	72.57	70.04	68.78
CLIP-hyp [†]	✗	71.87	69.58	65.31	63.95
CLIP-euc [†]	✗	71.61	69.00	64.69	63.28
CLIP	-	69.94	67.74	62.50	60.21

Table 6. **Part-based same-class image retrieval evaluation.** Cross-image ✓ indicates models fine-tuned on entailment relationships both within and across images at the category level, while ✗ represents models fine-tuned without cross-image sampling. The evaluation setup is the same as Table 1 in the main paper. The best results are marked in bold.

the validation set of the LVIS dataset [14], following the similar process as constructing *HierOpenImages*. To construct the ground truth hierarchy tree, we use the pipeline as described in Sec. A. We empirically choose parameter *frequency* = 5 and *proportion* = 5% in our experiments. This adjustment is necessary because the LVIS dataset [14] has very unbalanced classes.

Emergent structure. We observe that high-frequency, ambiguous image crops are naturally pushed toward the boundary of hyperbolic space, where more angular entailment constraints can be better satisfied. This aligns with the exponentially growing volume near the boundary, and it is an efficient solution for representing diverse, overlapping semantics. In Figure 10, in the left plot, the percentage of samples of the original *Sunglasses* crops are shown in dark green. Adding Gaussian blur or selecting extremely small crops shifts their embeddings further from the root. The small crops (red curve) are not included in other curves. The right plot shows clear separation between full and part image embeddings.

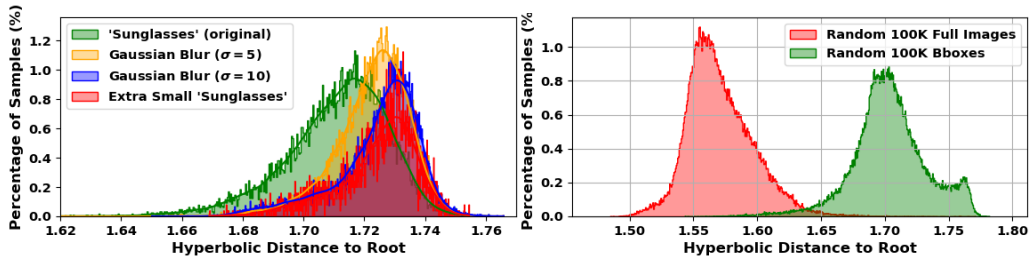


Figure 10. **Example of the model’s emergent structure.** In the left plot, the percentage of samples of the original *Sunglasses* crops are shown in dark green. Applying Gaussian blur or selecting extremely small crops shifts the embeddings further from the root. The right figure illustrates a clear separation between full-image and part-image embeddings.

Metrics	Model	Cross-Image	Top-150k	Top-200k	Top-250k
Recall % \uparrow	CLIP-hyp [†]	✓	77.00	85.75	91.89
	CLIP-euc [†]	✓	76.46	85.08	91.38
	CLIP-hyp [†]	✗	75.66	84.51	91.13
	CLIP-euc [†]	✗	75.22	84.15	91.10
	CLIP	-	66.63	77.15	86.57
OT Distance \downarrow	CLIP-hyp [†]	✓	14.96	17.57	20.76
	CLIP-euc [†]	✓	15.65	18.15	21.09
	CLIP-hyp [†]	✗	15.98	18.27	21.03
	CLIP-euc [†]	✗	16.19	18.46	21.02
	CLIP	-	21.31	22.74	23.79

Table 7. **Part-based hierarchical evaluation of parent-to-child image retrieval.** The OT distance is defined in Sec. 3.3 (main paper), and the evaluation setup follows Table 2 (main paper). The best results are marked in bold.

C. Ablation Studies

In this ablation study, we evaluate the impact of adding cross-image scene-to-object samples. We fine-tuned the CLIP ViT model solely on hierarchical part-based entailment data within individual images (entailment pairs with high visual similarity), excluding any cross-image image-to-bounding-box samples. The detailed results for same-class retrieval and hierarchical retrieval are presented in Table 6–7, with the best scores highlighted in bold. Overall, the results clearly show that incorporating cross-image samples further improves image retrieval performance.

D. More Qualitative Results

More qualitative parent-to-child retrieval results are shown in Fig. 11 to visualize the latent space. Bounding box images are filtered by angle (CLIP-

hyp[†]) or cosine similarity (CLIP ViT model) thresholds and sorted by increasing embedding norms. Our hyperbolic model retrieves diverse and visually distinct lower-level objects related to the query images, organized according to the predefined *scene-object-part* hierarchy in the embedding space.



Figure 11. **Example of parent-to-child retrieval using CLIP ViT and our CLIP-hyp[†] model.** Results are ordered by ascending embedding norms. Our model retrieves images matching the predefined *scene-object-part* hierarchy, placing high-level objects near the origin (e.g., group of fruits → single fruits), and grouping semantically related but visually distinct objects (e.g., chairs & TVs). All retrieved bounding box images are scaled to the same ratio.

Appendix

Object classes in LVIS dataset but not in OpenImage dataset

aerosol can	air conditioner	alcohol	alligator	almond	amplifier
anklet	antenna	applesauce	apricot	apron	aquarium
arctic	armband	armchair	armoire	armor	trash can
ashtray	asparagus	atomizer	avocado	award	awning
baboon	baby buggy	basketball back-board	bagpipe	baguet	bait
ballet skirt	bamboo	Band Aid	bandage	bandanna	banner
barbell	barrette	barrow	baseball base	baseball	baseball cap
basket	basketball	bass horn	bat	bath mat	bath towel
bathrobe	batter	battery	beachball	bead	bean curd
beanbag	beanie	bedpan	bedspread	cow	beef
beeper	beer bottle	beer can	bell	belt buckle	beret
bib	Bible	visor	binder	birdfeeder	birdbath
birdcage	birdhouse	birthday cake	birthday card	pirate flag	black sheep
blackberry	blackboard	blanket	blazer	blimp	blinker
blouse	blueberry	gameboard	bob	bobbin	bobby pin
boiled egg	bolo tie	deadbolt	bolt	bonnet	booklet
bookmark	boom microphone	bouquet	bow	bow	bow-tie
pipe bowl	bowler hat	bowling ball	boxing glove	suspenders	bracelet
brass plaque	bread-bin	breechcloth	bridal gown	broach	broom
brownie	brussels sprouts	bubble gum	bucket	horse buggy	horned cow
bulldog	bulldozer	bullet train	bulletin board	bulletproof vest	bullhorn
bun	bunk bed	buoy	business card	butter	button
cabana	cabin car	cabinet	locker	calendar	calf
camcorder	camera lens	camper	candle holder	candy bar	candy cane
walking cane	canister	canteen	cap	bottle cap	cape
cappuccino	railcar	elevator car	car battery	identity card	card
cardigan	cargo ship	carnation	horse carriage	tote bag	carton
cash register	casserole	cassette	cast	cauliflower	cayenne
CD player	celery	chain mail	chaise longue	chalice	chandelier
chap	checkbook	checkerboard	cherry	chessboard	chickpea
chili	chinaware	crisp	poker chip	chocolate bar	chocolate cake
chocolate milk	chocolate mousse	choker	chopstick	slide	cider
cigar box	cigarette	cigarette case	cistern	clarinet	clasp
cleansing agent	cleat	clementine	clip	clipboard	clippers
cloak	clock tower	clothes hamper	clothespin	clutch bag	coaster
coat hanger	coatrack	cock	cockroach	cocoa	coffee maker

coffeepot	coil	colander	coleslaw	coloring material	combination lock
pacifier	comic book	compass	condiment	cone	control
convertible	cooker	cooking utensil	cooler	cork	corkboard
corkscrew	edible corn	cornbread	cornice	cornmeal	corset
costume	cougar	coverall	cowbell	crabmeat	cracker
crape	crate	crayon	cream pitcher	crib	crock pot
crossbar	crouton	crow	crowbar	crucifix	cruise ship
police cruiser	crumb	cub	cube	cufflink	cup
trophy cup	cupcake	hair curler	curling iron	cushion	cylinder
cymbal	dalmatian	dartboard	date	deck chair	dental floss
detergent	diary	dinghy	dining table	tux	dish
dish antenna	dishrag	dishtowel	dishwasher detergent	dispenser	diving board
Dixie cup	dog collar	dollar	dollhouse	domestic ass	doorknob
doormat	dove	underdrawers	dress hat	dress suit	dresser
drill	drone	dropper	drumstick	duckling	duct tape
duffel bag	dumpster	dustpan	earphone	earplug	earring
easel	eclair	eel	egg	egg roll	egg yolk
eggbeater	eggplant	electric chair	elk	escargot	eyepatch
fan	ferret	Ferris wheel	ferry	fig	fighter jet
figurine	file	fire alarm	fire engine	fire extinguisher	fire hose
first-aid kit	fishbowl	fishing rod	flagpole	flamingo	flannel
flap	flash	fleece	flip-flop	flipper	flower arrangement
flute glass	foal	folding chair	footstool	forklift	freight car
French toast	freshener	frisbee	fruit juice	fudge	funnel
futon	gag	garbage	garbage truck	garden hose	gargle
gargoyle	garlic	gasmask	gazelle	gelatin	gemstone
generator	gift wrap	ginger	cincture	glass	globe
golf club	golfcart	gorilla	gourd	grater	gravestone
gravy boat	green bean	green onion	griddle	grill	grits
grizzly	grocery bag	gull	gun	hairbrush	hairnet
hairpin	halter top	ham	hammock	hamper	hand glass
hand towel	handcart	handcuff	handkerchief	handle	handsaw
hardback book	harmonium	hatbox	veil	headband	headboard
headlight	headscarf	headset	headstall	heart	heron
highchair	hinge	hockey stick	home plate	honey	fume hood
hook	hookah	hornet	hose	hot-air balloon	hotplate
hot sauce	hourglass	houseboat	hummingbird	hummus	icecream
popsicle	ice maker	ice pack	ice skate	igniter	inhaler
iron	ironing board	jam	jar	jean	jeep
jelly bean	jersey	jet plane	jewel	jewelry	joystick

jumpsuit	kayak	keg	kennel	key	keycard
kilt	kimono	kitchen sink	kitchen table	kitten	kiwi fruit
knee pad	knitting needle	knob	knocker	lab coat	lamb
lamb-chop	lamppost	lampshade	lanyard	laptop computer	lasagna
latch	lawn mower	leather	legging	Lego	legume
lemonade	lettuce	license plate	life buoy	life jacket	lightbulb
lightning rod	lime	lip balm	liquor	log	lollipop
speaker	machine gun	magazine	magnet	mail slot	mailbox
mallard	mallet	mammoth	manatee	mandarin orange	manager
manhole	map	marker	martini	mascot	mashed potato
masher	mask	mast	mat	matchbox	mattress
meatball	medicine	melon	microscope	milestone	milk can
milkshake	minivan	mint candy	mitten	money	monitor
motor	motor scooter	motor vehicle	mound	mousepad	music stool
nailfile	napkin	neckerchief	needle	nest	newspaper
newsstand	nightshirt	nosebag	noseband	notebook	notepad
nut	nutcracker	oar	octopus	octopus	oil lamp
olive oil	omelet	onion	orange juice	ottoman	overalls
packet	inkpad	pad	padlock	paintbrush	painting
pajamas	palette	pan	pan	pantyhose	papaya
paper plate	paperback book	paperweight	parakeet	parasail	parasol
parchment	parka	passenger car	passenger ship	passport	patty
pea	peanut butter	peeler	wooden leg	pegboard	pelican
pencil	pendulum	pennant	penny	pepper	pepper mill
persimmon	pet	pew	phonebook	phonograph record	pickle
pickup truck	pie	pigeon	piggy bank	pin	pinecone
ping-pong ball	pinwheel	tobacco pipe	pipe	pita	pitcher
pitchfork	place mat	playpen	pliers	plow	plume
pocket watch	pocketknife	poker	pole	polo shirt	poncho
pony	pop	postbox	postcard	pot	potholder
pottery	pouch	power shovel	projector	propeller	prune
pudding	puffer	puffin	pug-dog	puncher	puppet
puppy	quesadilla	quiche	quilt	race car	radar
radiator	radio receiver	raft	rag doll	raincoat	ram
raspberry	rat	razorblade	reamer	rearview mirror	receipt
recliner	record player	reflector	rib	ring	river boat
road map	robe	rocking chair	rodent	roller skate	Rollerblade
rolling pin	root beer	router	rubber band	runner	saddle
saddle blanket	saddlebag	safety pin	sail	salad plate	salami
salmon	salmon	salsa	saltshaker	satchel	saucepan
sausage	sawhorse	scarecrow	school bus	scraper	scrubbing brush

seabird	seaplane	seashell	shaker	shampoo	sharpener
Sharpie	shaver	shaving cream	shawl	shears	shepherd dog
sherbert	shield	shoe	shopping bag	shopping cart	shot glass
shoulder bag	shovel	shower head	shower cap	shower curtain	shredder
signboard	silo	skewer	ski boot	ski parka	ski pole
skullcap	sled	sleeping bag	sling	slipper	smoothie
soap	soccer ball	softball	solar array	soup	soup bowl
soupspoon	sour cream	soya milk	space shuttle	sparkler	spear
crawfish	sponge	sportswear	spotlight	stagecoach	statue
steak	steak knife	steering wheel	stepladder	step stool	stereo
stew	stirrer	stirrup	brake light	stove	strainer
strap	street sign	streetlight	string cheese	stylus	subwoofer
sugar bowl	sugarcane	sunflower	sunhat	mop	sweat pants
sweatband	sweater	sweatshirt	sweet potato	Tabasco sauce	table-tennis table
table lamp	tablecloth	tachometer	tag	taillight	tambourine
army tank	tank top	tape	tape measure	tapestry	tarp
tartan	tassel	tea bag	teacup	teakettle	telephone booth
telephone pole	telephoto lens	television camera	television set	tequila	thermometer
thermos bottle	thermostat	thimble	thread	thumbtack	tights
timer	tinfoil	tinsel	tissue paper	toast	toaster oven
tongs	toolbox	toothpaste	toothpick	cover	tortilla
tow truck	towel rack	tractor	dirt bike	trailer truck	trampoline
tray	trench coat	triangle	tricycle	truffle	trunk
vat	turban	turnip	turtleneck	typewriter	underwear
urinal	urn	vacuum cleaner	vending machine	vent	vest
videotape	vinegar	vodka	volleyball	vulture	wagon
wagon wheel	walking stick	wall socket	wallet	walrus	washbasin
water bottle	water cooler	water heater	water jug	water gun	water ski
water tower	watering can	weathervane	webcam	wedding cake	wedding ring
wet suit	whipped cream	whistle	wig	wind chime	windmill
window box	windshield wiper	windsock	wine bottle	wine bucket	wineglass
blinder	wolf	wooden spoon	wreath	wristband	wristlet
yacht	yogurt	yoke			